View metadata, citation and similar papers at core.ac.uk
brought to you by CORE
provided by DSpace at VU

Solvation Effects on the S_N2 Reaction between CH_3Cl and Cl^- in Water

Bernd Ensing,[†] Evert Jan Meijer,[‡] P. E. Blöchl,[§] and Evert Jan Baerends*[,†]

Theoretical Chemistry, Faculty of Sciences, Vrije Universiteit Amsterdam, De Boelelaan 1083, NL-1081 HV Amsterdam, The Netherlands, Department of Chemical Engineering, Universiteit van Amsterdam, Nieuwe Achtergracht 166, NL-1018 WV Amsterdam, The Netherlands, and IBM Research Division, Zurich Research Laboratory, Saumerstrasse 4, Rüschlikon, CH 8803, Zurich, Switzerland

Received: September 25, 2000

Car−Parrinello molecular dynamics simulations have been performed to investigate the solvation effects on the prototype S_N2 reaction between Cl^- and CH_3Cl. The free energy barrier for this reaction in water was calculated using constrained dynamics at a constant temperature of 300 K and constant volume. Calculations on the isolated system (reaction in the gas phase at zero temperature) were performed for reference purposes. Qualitatively, the calculations confirm that the double-well free energy profile of the reaction in the gas phase is converted into a single barrier by solvation and that the height of the barrier increases significantly. Quantitatively, there are two error sources. At the electronic structure side, the Becke−Perdew functional underestimates the barrier height by 8 kcal/mol. At the dynamics side, there is a "hysteresis" effect—too slow an adaptation of the solvent structure to changes in the reaction coordinate—yielding an estimated error of 3 kcal/mol in the free energy barrier height. After correction for these errors, the calculated value of the free energy barrier is 27 kcal/mol. Considering the accuracy of the solvent−solvent and solvent−reactant interactions of ca. 1 kcal/mol, this compares very well with the experimental estimate of 26.6 kcal/mol. This indicates that the ab initio (DFT) MD very well captures the differential energetic as well as entropic effects of the solvation when going from the (solvated) reactants to the initial ion−dipole complex to the transition state.

I. Introduction

The presence of solvent can have a major impact on the thermodynamics and kinetics of chemical reactions. Aspects such as electrostatic interactions and steric hindrance can play an important role in this respect. Also, chemical binding of solvent molecules to the reacting species may have a strong effect. A detailed microscopic picture of these effects is of fundamental interest and provides insight for possible improvements with respect to the rate, balance, and selectivity of chemical reactions.

Molecular simulation is an appropriate tool to obtain such a detailed picture. A high-level quantitative molecular simulation of a chemical reaction in solution requires the use of accurate quantum chemical methods to describe the change in chemical bonding, in combination with a statistical mechanical description of the effect of the rearrangement of solvent molecules. The Car−Parrinello (CP) method[1] satisfies these two requirements in a computationally efficient manner. It combines density functional theory (DFT) to describe the electronic structure with molecular dynamics (MD) to incorporate the motion of the molecules. The forces on the molecules that govern their motion are obtained directly from the electronic structure calculation. Therefore, the method may be regarded as an ab initio (DFT) molecular dynamics (AIMD) simulation. Of particular importance for the present work is that AIMD has proven to be applicable to the study of the structure and dynamics of water[2−5] and simple chemical reactions in aqueous solution.[6,7]

The purpose of the present study is to gain microscopic insight in the energetics, mechanism, and structural aspects of the solvation effects on a prototype S_N2 reaction in water, with a minimal level of approximation and without the use of empirical data. In particular, we have investigated the effect of solvation in a dilute aqueous HCl solution of the bimolecular nucleophilic substitution (S_N2) reaction.

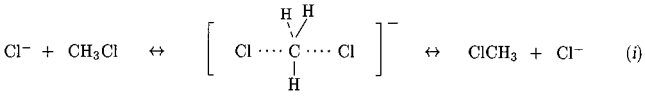

The S_N2 type of reaction is one of the most fundamental processes in organic chemistry and has been the subject of numerous theoretical[8−13] and experimental studies.[14−16] The energy profile for the gas-phase reaction between methyl chloride and a chloride anion is commonly believed to have a symmetrical double-well shape, with the two minima related to the ion−dipole complexes centered around a maximum at the transition state. However, experimental evidence shows that in aqueous solution the profile is unimodal and the reaction rate much lower compared to that of the gas-phase reaction. Using classical Monte Carlo simulations, Chandrasekhar, Smith, and Jorgensen[17] were the first to compute the barrier for the $Cl^- + CH_3Cl$ reaction in aqueous solution. They developed model potentials for the interactions between the water molecules and the solutes (Cl^- and CH_3Cl) and among water molecules by fitting to ab initio calculations. It is an advantage of the Car−Parrinello simulation that these potentials are obtained directly. This is particularly important in a case like the present one, where construction of good model potentials is difficult because

* Corresponding author.
[†] Vrije Universiteit Amsterdam.
[‡] Universiteit van Amsterdam.
[§] Zurich Research Laboratory.

10.1021/jp003468x CCC: $20.00 © 2001 American Chemical Society
Published on Web 03/01/2001

of the changes in the charges on the attacking and leaving chloride ions, and hence in their solvation, along the reaction coordinate.

The reaction studied in the present work is activated. The experimental value for the activation energy is 27 kcal mol^{-1}.[18] A successful reaction is therefore a rare event and outside the time scale accessible to ab initio molecular dynamics. To study such reactions by MD, we must force a reactive encounter on the system by some form of microscopic control of a suitable reaction coordinate. This is achieved by using the method of constraint that allows for the evaluation of the free energy profile along the reaction path.[19]

This paper is organized as follows: In section II, we describe the computational details of the DFT and MD method, the method of constrained dynamics to calculate the reaction free energy, and the relevant parameters for the gas phase and aqueous solution calculations. Section III starts with the results of some preparatory simulations that serve to assess the accuracy of the methods used. The simulation results of the S_N2 reaction in gas phase and in aqueous solution are presented in subsections III.C and III.D, respectively. In section IV, a discussion of our results for the solvation effect on the reaction barrier is given, and we end with conclusions in section V.

II. Method

A. Density Functional and Molecular Dynamics Method. The electronic structures were computed using density functional theory (DFT) (see, e.g., ref 20). For the exchange−correlation functional we used the Perdew−Zunger[21] parametrization of the local density approximation (LDA) for this functional, which is based on the free electron MC simulations by Ceperley and Alder.[22] Density gradient corrections were added, namely, the Becke-88 gradient correction for exchange[23] and the Perdew-86 gradient correction for correlation.[24]

The Car−Parrinello (CP) method[1] was applied to perform both dynamic and static calculations. The method performs the classical MD and simultaneously applies DFT to describe the electronic structure, using an extended Lagrangian formulation. The characteristic feature of the Car−Parrinello approach is that the electronic wave function, i.e., the coefficients of the plane wave basis set, are dynamically optimized to be consistent with the changing positions of the atomic nuclei. The actual implementation involves the numerical integration of the equations of motion of second-order Newtonian dynamics. A crucial parameter in this scheme is the fictitious mass m_e associated with the dynamics of the electronic degrees of freedom. In practice, m_e has to be chosen small enough to ensure fast wave function adaptation to the changing nuclear positions on one hand and sufficiently large to have a workable large time step on the other. In the present work, the equations of motion were integrated using the Verlet[25] algorithm with a mass $m_e = 1000$ au $= 910\,939\,10^{-28}$ kg, which limits the time step to $\delta t = 0.19$ fs. To maintain a constant temperature of $T = 300$ K, we applied a Nosé thermostat[26] with a period of 100 fs.

The CP simulations have been performed using the CP-PAW code package developed by Blöchl. It implements the ab initio molecular dynamics together with the projector augmented wave (PAW) method.[27] The PAW method uses an augmented plane wave basis for the electronic valence wave functions and, in the current implementation, frozen atomic wave functions for the core states. Thus, it is able to produce the correct wave function and densities also close to the nucleus, including the correct nodal structure of the wave functions. The advantages compared to the pseudopotential approach are that transferability problems are largely avoided, that quantities such as hyperfine parameters and electric field gradients are obtained with high accuracy,[28,29] and, most important for the present study, that a smaller basis set as compared to traditional norm-conserving pseudopotentials are required. The frozen core approximation was applied for the 1s electrons of C and O and up to 2p for Cl. For H, C, and O, one projector function per angular-momentum quantum number was used for *s*- and *p*-angular momenta. For Cl, two projector functions were used for *s*-angular momenta and one for *p*-angular momenta. The Kohn−Sham orbitals of the valence electrons were expanded in plane waves up to a kinetic energy cutoff of 30 Ry.

For reference, we also performed static DFT calculations using the atomic-orbital based ADF package.[30] In these calculations, the Kohn−Sham orbitals were expanded in an uncontracted triple-ζ Slater-type basis set augmented with one 2p and one 3d polarization function for H, 3d, and 4f polarization functions for C, O, and Cl.

B. Free Energy Calculation. The equilibrium constant and the transition-state theory estimate of the reaction rate of a chemical reaction are determined by the free energy profile along the reaction path. The free energy reaction barrier is the reversible work necessary to bring the system from the stable state of reactants (RS) to the transition state (TS). We will characterize these states by some order parameter, a reaction coordinate ξ, which is a function of the positions of the nuclei. As the reversible work is independent of the path, the precise choice of the reaction coordinate is not crucial, but a practical and physically appealing choice is one that incorporates the asymmetric stretch vibration along the Cl−C−Cl axis of the transition-state complex CH_3Cl_2. Given a choice for the reaction coordinate, we can obtain the free energy change $\Delta A(\xi)$ along the reaction path using the technique of thermodynamic integration (see, e.g., ref 31)

$$\Delta A(\xi) = \int_{\xi RS}^{\xi} \left\langle \frac{\partial H}{\partial \xi} \right\rangle_{\xi'} \mathrm{d}\xi' \qquad (1)$$

Here H is the Hamiltonian of the system of nuclei, defined as the sum of the kinetic and (Born−Oppenheimer) potential energy, and, minus the integrand $-\langle \partial H/\partial \xi \rangle$, is usually called the mean force. The brackets denote an ensemble average, and the subscript indicates that the integrand is evaluated at the point $\xi(\mathbf{r}) = \xi'$ along the reaction coordinate, where $\mathbf{r}$ denotes the total of nuclear coordinates.

The S_N2 reaction studied in the present work is an activated process, which implies that the barrier is too high for the reaction to take place spontaneously within the time scale accessible to an MD simulation. The probability of finding the system close to the transition state is very small, and the reaction is therefore a rare event. To nevertheless be able to estimate the mean force at the reaction coordinate values of low probability, we can use the method of constraint where the dynamics of the system is performed with the reaction coordinate fixed at a specified value ξ'. The theoretical framework of the study of activated processes in an MD simulation has been established some time ago in ref 32 and also ref 19, which provided a microscopic expression for the mean force. An approximate version of this method,[33,34] only valid for reaction paths controlled by special classes of constraints, has been successfully used in quite a number of simulations of reactions.[6,35,36] More recently, generally applicable expressions for the mean force have been outlined,[37,38] which include the explicit terms to correct for the bias introduced in the ensemble by applying the constraint (see also the appendix).

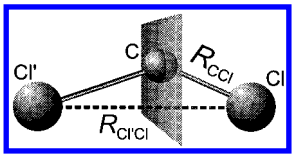

Figure 1. Geometry parameters defining the reaction coordinate (equation 2). One characteristic of the chosen reaction coordinate is that for a particular value of the coordinate, the carbon is allowed to move only in a plane perpendicular to that of the line through the chlorine atoms.

The reaction coordinate used in the present study is defined as the normalized projection of the C−Cl bond R_{CCl} on the Cl′−Cl bond $R_{Cl'Cl}$ (see Figure 1)

$$\xi = \frac{R_{CCl}\cos(\angle_{CClCl'})}{R_{ClCl'}} \tag{2}$$

Here $\angle_{CClCl'}$ is the angle between the C−Cl and Cl′−Cl bonds. In the following, we will refer to Cl′ and Cl as the attacking and leaving chloride, respectively. Since the reaction is symmetric, the transition state is at a point where both C−Cl distances are equal. At this transition state, the value of the reaction coordinate (eq 2) is $\xi = 0.5$, whereas it approaches zero for separated reactants and one for separated products.

C. Gas-Phase Computations. The CP-PAW calculations of the isolated compounds were performed in a cubic periodic unit cell of size $L = 10$ Å. A rectangular periodic unit cell of size $10 \times 10 \times 18$ Å was used for the isolated (gas phase) reaction. These sizes are sufficiently large to ensure negligible overlap of the wave functions of the periodic images. To suppress the electrostatic interaction among the periodic images, we used the method of electrostatic decoupling of ref 39.

For the ADF calculations, the finite-temperature reaction enthalpies at $T = 300$ K and the entropies were estimated using

$$\Delta H_{300K} = \Delta E_0 + \Delta E_{ZPE} + \Delta E_T^v + \Delta E^t + \Delta E^r + \Delta(PV) \tag{3}$$

$$\Delta S = R \ln(Q^t Q^r Q^v) \tag{4}$$

with E_0 being the sum of the electronic energy in a static nuclear field (Born−Oppenheimer approximation) and the nuclear electrostatic repulsion. The zero-point vibrational energy E_{ZPE} and the temperature-dependent vibrational energy E_T^v were calculated from the unscaled DFT-BP frequencies, within the harmonic approximation. The change in translational energy ΔE^t, rotational energy ΔE^r, and PV were obtained using the ideal gas law, associating $^1/_2 k_B T$ to each degree of freedom. The partition function Q is the product of translational, rotational and vibrational contributions (see, e.g., chapter 20 in ref 40).

D. Aqueous Solution Computations. We performed Car−Parrinello molecular dynamics simulations of the following solutions: (a) HCl in water, (b) CH_3Cl in water, and (c) both HCl and CH_3Cl in water. For reference, a CP-PAW calculation of a pure water sample of 32 H_2O molecules per unit cell was also done (d). All simulations were performed in a periodic system with the cubic unit cell containing one of each type of solute molecules (HCl or CH_3Cl or both) and 32 water molecules. The box sizes were 9.9684, 10.1450, 10.2463, and 9.8650 Å for samples a, b, c, and d, respectively, yielding the experimental density of the solution at $T = 300$ K. The simulations of sample c, the reactants in water, yield the central result of the present work. It involved the calculation of the free energy barrier for the $CH_3Cl + Cl^-$ reaction in water by a series of constrained CP-PAW runs at different values of the reaction coordinate (eq 2). The starting configuration of the first run was created from a previous run of CH_3Cl in water (sample b) at 300 K. A sphere-shaped cavity of radius 2 Å was created near the CH_3Cl molecule, in which HCl′($R_{HCl'} = 1.10$ Å) was placed at a distance from CH_3Cl equal to $R_{CCl'} = 4.00$ Å and with an angle $\angle_{HCl'C} = 180°$. With the angle $\angle_{ClCCl'} = 176°$ and the C−Cl distance in CH_3Cl $R_{CCl} = 1.871$ Å, this corresponds to a value for our reaction coordinate in this initial snapshot of $\xi = 0.318\,48$. This value was constrained, and equilibration was performed at $T = 300$ K until there was no longer a drift in the constraint force and the potential energy $E[\rho]$. Then a production run of 3−5 ps was performed to collect statistics. After each production run, the constraint was moved to the next reaction coordinate value in a number of steps large enough to keep the induced atomic velocities very small compared to their average velocities at $T = 300$ K (typically 1000−2000 steps). This was again followed by equilibration and mean force sampling. Equilibrations took typically 1.5−3 ps.

III. Results

In this section, we will present (1) reference calculations to assess the accuracy of the DFT approach and its implementation in the CP-PAW code and (2) the results of calculations of a sample of 32 water molecules of pure water and the solvation of a single HCl molecule (i.e., the samples referred to as a and d in the previous section D). These calculation serve as a validation of the theoretical approach and numerical methods used. Subsequently, we present the results of the gas-phase S_N2 reaction *i* and the results of the CP-PAW calculations of the S_N2 in water.

A. Structures and Energies of Isolated Compounds. To test the accuracy of the DFT approach and the CP-PAW package, we performed geometry optimizations of four small molecules and two small complexes (water dimer and water−chloride complex) relevant to reaction *i*.

We optimized the structures of Cl_2, HCl, H_2O, and CH_3Cl with the CP-PAW program and compared these with results obtained with the ADF package and literature values. The results of the geometry optimizations are compiled in Table 1. The first two columns show our PAW results with two different plane wave basis sets.

The geometry appears to be practically converged at the plane wave cutoff of 30 Ry. The largest bond distance discrepancy between the 30 Ry and the large 50 Ry basis set are found for R_{OH} and R_{CH}, namely, 0.006 Å. Comparing the CP-PAW and ADF results, there are larger differences. The largest discrepancy is found for the R_{CCl} (0.024) and R_{ClCl} (0.042) distances. After the simulations had been done, we were able to trace the differences to the limited number of projector functions for Cl in the PAW method. Increasing the set of projector functions leads to very good agreement with the ADF results. Given the experimental uncertainties, the accuracy of the present CP-PAW results with the smaller set of projectors are satisfactory for our purposes. Bond lengths are slightly overestimated, with the largest errors for R_{CCl} being 0.077 Å and for R_{ClCl} being 0.047 Å. Angles are correct within 1°.

Atomization energies obtained with CP-PAW are converged within 0−2 kcal/mol at a plane wave cutoff of 30 Ry. The differences between the CP-PAW energies and the ADF ones are somewhat larger, from 1 to 4 kcal/mol.

The water dimer H_2O-H_2O and the H_2O-Cl^- complex served as a second validation of CP-PAW. The water dimer has been extensively used as a test model for the hydrogen bond

TABLE 1: Comparison of Bonding Energies (kcal/mol) and Geometries (Å and deg) Calculated with the CP-PAW Program and the ADF Program with Other Calculations and Experiment

molecule	property	PAW BP/30Ry	PAW BP/50Ry	ADF BP/TZDP	B3LYP[a] 6-31G*	G2[b] MP2/6-31G*	exp.[c]
Cl_2	ΔE_{Bond}	−58.2	−58.2	−62.3		−56.56	58.0
	R_{ClCl} [Å]	2.065	2.065	2.023	2.042	2.015	1.988[d]
HCl	ΔE_{Bond}	−105.7	−106.0	−107.8		−106.7	106.3
	R_{HCl} [Å]	1.308	1.304	1.293	1.290	1.280	1.275[e]
H_2O	ΔE_{Bond}	−232.59	−234.46	−237.88		−232.5	232.2
	R_{OH} [Å]	0.985	0.979	0.971	0.969	0.969	0.957[f]
	$\angle_{HOH}$ [°]	103.77	104.09	104.07	103.6	104.0	104.4[f]
CH_3Cl	ΔE_{Bond}	−401.9	−404.2	−402.2		−394.8	393.8
	R_{CH} [Å]	1.102	1.096	1.093	1.090	1.088	1.08[g]
	R_{CCl} [Å]	1.827	1.827	1.803	1.803	1.777	1.78[g]
	$\angle_{HOCl}$ [°]	107.9	107.8	108.3	108.5	108.9	108.2[g]

[a] B3LYP 6-31G* geometries from ref 61. [b] G2 energies (effectively, QCISD(T)/6-311+G(3df,2p) level) based on MP2/6-31G* geometries from ref 61. [c] Experimental bonding energies minus the zero-point energy correction from refs 62 and 63. [d] Ref 64. [e] Ref 65. [f] Ref 66. [g] Ref 67.

TABLE 2: Water Dimer Bonding Energy (kcal/mol) and Geometry (deg and Å) Calculated with PAW (two different plane wave cutoffs) and ADF Compared to Other Car−Parrinello Calculations and Accurate DFT, ab Initio, and Experimental Results

	$\Delta E_{intermol}$	R_{OO}	R_{OH_b}	R_{H_bO}	$\angle_{OHO}$
PAW−BP 30Ry	−4.49	2.954	0.997	1.962	173.3
PAW−BP 50Ry	−4.35	2.938	0.990	1.955	171.6
ADF−BP/TZDP	−4.94	2.893	0.982	1.916	172.8
CPMD-BP 70Ry[a]	−4.5	2.95			177
CPMD-BP 150Ry[a]	−4.3	2.94			177
DFT-BP/aug-cc-pVDZ*[b]	−4.69	2.886	0.985	1.908	172
DFT-BP/TZVP[c]	−4.69	2.885			
DFT-BLAP3/TZVP[c]	−4.63	2.979			
DFT-PLAP3/TZVP[c]	−4.68	2.950			
DFT-HCTH38/TZ2P[d]	−4.60	2.952			
DFT-B3LYP/aug-cc-pVTZ[b]	−4.57	2.917	0.970	1.953	172
DFT-B3PWa[e]	−3.629	2.950	0.962		
MP2[f]	−4.995	2.917	0.966	1.958	172
CASSCF/aug-cc-pVDZ[g]		3.084	0.948	2.143	172
CCSD(T)[h]	−4.98	2.925			175.7
CCSD(T)[i]	−4.96	2.895			
exp.	-5.4 ± 0.7[j]	2.946[k]			174[l]
	-5.4 ± 0.2[m]	2.952[n]			

[a] CP simulations with a norm conserving pseudopotential and 70 and 150 Ry plane wave cutoff.[3] [b] Ref 43. [c] Ref 44. [d] GGA fitted to a set including the water dimer, BSSE-corrected.[68] [e] Beckes hybrid exchange + Perdew−Wang correlation parametrized also for the water dimer, BSSE-corrected.[69] [f] ΔE from ref 70 (MP2, 444 AOs, CP-corrected) and geometry from ref 60 (frozen core, counterpoise-corrected); one of the many accurate MP2 results (see text). [g] Complete active space of 16 electrons in 12 orbitals (35 793 configuration state functions) computation from ref 71. [h] Ref 58. [i] Halkier et al[42] (aug-cc-pVTZ, frozen core, rigid monomers). [j] Ref 72. [k] Experimental microwave result for $R_{0,OO}$ (2.976 Å) corrected for anharmonicy from ref 73. [l] Ref 74. [m] Ref 75. [n] Another anharmonicy correction[76] bases on the experiment of Ref 73.

description. A small selection of literature data and our results are compiled in Table 2. Large basis set MP2 calculations yield an interaction energy of $\Delta E = -5.0$ kcal/mol[41] and an oxygen−oxygen distance of $R_{OO} = 2.92$ Å. The best theoretical estimates are probably given by the CCSD(T)/aug-cc-pVTZ calculation of Halkier et al.[42] extrapolating for the CCSD(T) limit to $R_{OO} = 2.90$ Å and $\Delta E = -5.0 \pm 0.1$ kcal/mol and also the CCSD(T) results by Schütz et al. ($R_{OO} = 2.925$ Å and $\Delta E = -4.98 \pm 0.02$ kcal/mol) and Klopper et al. ($\Delta E = -5.057$ kcal/mol). The discrepancy of the experimental results ($\Delta E^{exp} = -5.4 \pm 0.2$ kcal/mol, $R_{OO}^{exp} = 2.95$ Å) with these results is attributed by Schütz et al. to an underestimation of the anharmonicy corrections in the experimental result.

Compared to the high-level ab initio results, the computationally less demanding DFT methods yield similar results. Our CP-PAW results agree very well with the work of Sprik, Hutter, and Parrinello,[3] who recommended the BP (and BLYP) functional for water simulations. If the larger plane wave basis set of 50 Ry is used, the CP-PAW result for ΔE is 0.34 kcal/mol less negative than the BP/aug-cc-pVDZ result of Kim and Jordan[43] and the BP/TZVP work of Proynov, Sirois, and Salahub.[44] Our ADF computation results in a 0.25 kcal/mol stronger interaction. The advanced BLAP3 functional (which combines Beckes GGA exchange functional[45] with the 4-parameter LAP3 correlation functional, which includes also second order derivatives of the density) returns virtually the same interaction energy as that of BP. Note that the oxygen−oxygen bond length is overestimated with BLAP3 even though the water dimer was included in the parameter fitting set. Using the Perdew−Wang exchange functional[46] in combination with LAP3 gives $R_{OO} = 2.950$ Å.[44] We conclude that for the water dimer CP-PAW gives satisfactory results for our purposes.

A molecular simulation of the S_N2 reaction *i* involves the solvation of CH_3Cl, Cl^-, and $[Cl\cdots CH_3\cdots Cl]^-$. An accurate simulation requires therefore a good description of the strong hydrogen bonds between water and the electronegative chlorine compounds. Combariza and Kestner[47] have pointed out that proposed empirical force fields for this interaction seem to have serious deficiencies. This is reflected in inaccurate geometries for small clusters $Cl^-(H_2O)_n$ when compared to experimental evidence and correlated quantum chemical calculations on the MP2 or DFT level.

Here we will just consider the simplest ($n = 1$) $H_2O\cdots Cl$ complex. Results are listed in Table 3. The CP-PAW result for the interaction energy is 0.64 kcal/mol less than the prediction of ADF, and the largest geometry difference is found for the R_{OCl^-} equal to 0.031 Å. DFT-BP slightly overestimates the interaction when compared to that of the experiment and performs on the same level as that of DFT-B3LYP and MP2/MP4. The angle $\angle_{OHCl^-}$ found with DFT-BP agrees within 1° with other theoretical methods methods.

The overall conclusion is that for the water−water and water−anion interactions, CP-PAW provides a sufficiently accurate DFT-BP result. In turn, DFT-BP performs as well as MP2/MP4/B3LYP, and the results are all close to the experimental data.

B. Water and Hydrochloric Acid. The last two test cases, before actually treating the S_N2 reaction, deal with CP-PAW molecular dynamics simulations of water and hydrochloric acid (HCl) in water (i.e., cases a and d in section II.D). The pure water sample consisted of 32 water molecules in a periodic cubic box with an edge of 9.8650 Å, which was taken from a previous empirical force-field MD simulation. After equilibrating for 15

TABLE 3: Water−Chloride Bonding Energy (kcal/mol) and Geometry (Å and Deg) Calculated with CP-PAW and ADF and Compared to Other Method

	$\Delta E_{\text{intermol}}$	R_{HCL^-}	R_{OH}	$R_{\text{OH}'}$	R_{OCl^-}	$\angle_{\text{OHCl}^-}$	$\angle_{\text{HOH}'}$
CP-PAW−BP/30Ry	−15.48	2.090	1.028	0.984	3.115	174.9	101.6
ADF−BP/TZDP	−16.12	2.075	1.014	0.970	3.084	173.0	100.9
DFT-P86/DZVP[a]		2.15	1.01	0.98			
DFT-BLYP[b]	−14.2	2.16	0.99	0.96	3.15	168.66	101.39
MP2/aug-cc-pVTZ[c]	−14.6	2.116	0.991	0.961	3.094	168.9	100.6
MP4/aug-cc-pVTZ[c]	−14.54	2.125	0.991	0.963	3.103	168.7	100.7
exp.	−15.2[d] to −15.0[e]						

[a] Ref 77 (the type of exchange functional remains unclear in the article). [b] DFT results using a 6-31++G(3 *d*, *p*) basis on water and for Cl^- the basis set of McLean and Chandler augmented with diffuse *sp*- and *d*-functions, from ref 47. [c] BSSE-corrected results from Xantheas.[78] [d] $\Delta H = -14.7 \pm 0.6$ kcal/mol from the mass spectroscopy results from ref 79 minus the zero-point energy correction of $\Delta E^{\text{ZPE}} = 0.3$ kcal/mol from ref 78. [e] $\Delta H = -14.9$ both found by Sieck[80] and Yamabe et al.[81] using mass spectroscopy minus $\Delta E^{\text{ZPE}} = 0.3$ kcal/mol.[78]

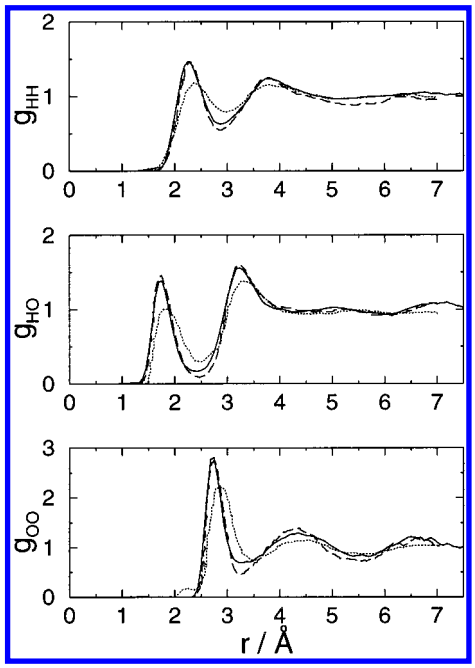

Figure 2. Radial distribution of water at $T = 300$ K (solid lines) compared to the Car−Parrinello simulation from ref. 3 (dashed lines) and the neutron diffraction data from ref 88 (dotted lines).

ps to obtain natural distributions for the atomic positions and velocities at $T = 300$ K, we computed a trajectory of 8.6 ps, from which some structure and dynamics parameters for liquid water were calculated. The hydrochloric acid sample was obtained from the equilibrated water sample by inserting one HCl molecule and scaling the cubic box up to an edge of 9.9684 Å to yield the experimental density of a 1:32 ratio of HCl to H_2O molecules (1.66M) solution. The equilibration time for the HCl and 32 water molecules system was 10 ps and the following 7.7 ps of trajectory was again used for analysis.

The calculated radial distribution functions of the pure water sample are shown in Figure 2. As expected, our results obtained using the CP-PAW method are very similar to the CP-MD results by Sprik, Hutter, and Parrinello,[3] with a small discrepancy in the depth after the first peak in g_{OO}. When compared to neutron diffraction data, the peak values are overestimated, and their positions shifted to smaller radii. The overall resemblance of the radial distribution is satisfactory, where we note that DFT-BP has a tendency to enhance structure of the liquid, as concluded earlier in ref 3. The peak positions and coordination numbers are listed in Table 4. In view of the experimental numbers quoted for the coordination numbers, this seems to be a quantity that is difficult to measure. Nevertheless, it can be seen from the table that the CP-PAW simulation underestimates the H_2O coordination somewhat. Comparing the CP-PAW

TABLE 4: Some Properties of Liquid Water Compared[a]

	R_{OH}	$n_{\text{c OH}}$	R_{OO}	$n_{\text{c OO}}$	D
CP-PAW	1.73	1.78	2.72	4.10	1.3 ± 0.7
SHP[b]			2.72	3.9 ± 0.2	$0.35 \pm 30\%$
MC/MD(TIP4p)	1.9[c]	1.9[c]	2.75[d]	5.1[c]	3.3 ± 0.5[e]
MD(SSD)[g]	1.9	2.0	2.75	5.2	$2.24 \pm 2\%$
X-ray[h]			2.7−2.8	4.3	

[a] Peak maxima R_{OH} and R_{OO} are given in Å. The coordination numbers $n_{\text{c OH}}$ and $n_{\text{c OO}}$ were estimated for all methods by integration of the first peak of g_{OH} and g_{OO} up to the next minimum (at, respectively, 2.3/3.25 Å for the AIMD results and 2.5/3.5 Å for the other methods). The experimental self-diffusion coefficient D is 2.35 cm^2/s.[82] [b] Ref 3 using Car−Parrinello MD simulations. R_{OO} was read from the graph. [c] From Figure 1 in ref 83. [d] MD/TIP4 (transferable intermolecular potential-4 points) results from ref 84. [e] MD/TIP4 results from ref 85. [f] MD/SSD (soft sticky dipole model) results from refs 86 and 87. [g] Ref 88 using neutron diffraction. [h] Refs 89 and 90 using X-ray diffraction.

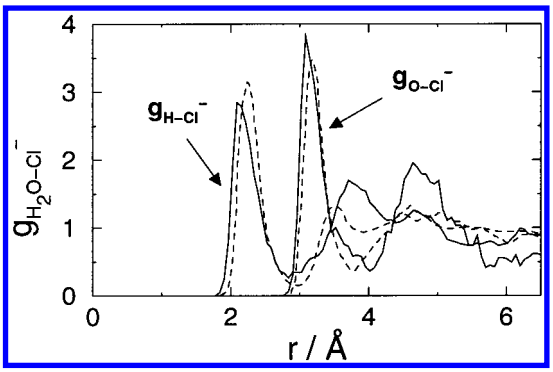

Figure 3. Radial distribution around Cl^- at $T = 300$ K (solid lines) compared to the MD results using a polarizable semiempirical force field from ref 52 (dotted lines).

calculations to MD results obtained using the TIP4P or SSD force fields shows similar values for the O−O peak position. However, force field results for the O−H peak position and the coordination numbers are larger than the CP-PAW results.

The self-diffusion coefficient D in the pure water sample was calculated from the mean-square displacement. Due to the short simulated trajectory of 8.6ps, the statistical error, estimated from 1 ps block averages, is relatively very high. Our result of $D = 1.3 \pm 0.7$ cm^2/s lies between the experimental value[48] of $D^{\text{exp}} = 2.35$ cm^2/s and the value of $D^{\text{AIMD}} = 0.35 \pm 0.1$ cm^2/s from the CP-MD simulation of ref 3.

The results of the CP-PAW MD simulation of the dilute aqueous HCl solution are summarized in Figure 3 and Table 5 that show the Cl−H and Cl−O radial distribution functions and list the distribution peak positions and estimated coordination numbers, respectively.

AIMD simulations of aqueous HCl solutions have been reported earlier by Laasonen and Klein.[49,50] They considered

TABLE 5: Structural Parameters of Cl^- in Water Compared with Other Molecular Simulation Results and Experiment

	R_{Cl^-H}	$n_{c\,Cl^-H}$	R_{Cl^-O}	$n_{c\,Cl^-O}$
CP-PAW	2.11	5.2	3.09	6.5 (7.2)[a]
MC/TIP4p[b]	2.25	7.0	3.21	7.4
MD/TIP4p[c]	2.34	7.0	3.27	7.2
MD/pol.[d]	2.25	5.9	3.18	6.1
neutr. diff.[e]	2.22−2.26	−	3.20−3.34	5.3−6.2
X-ray[f]	−	−	3.10−3.35	5−11

[a] Peak integrated up to $r = 3.75$ Å as in the literature. Peak in parentheses integrated up to the $g(r)$ minimum at $r = 4.0$ Å. [b] Ref 51 using Monte Carlo simulations with the TIP4p potential. [c] Ref 52 using molecular dynamics simulations with the TIP4p potential. [d] Ref 53 using molecular dynamics simulations with a polarizable model. [e] Ref 91 using neutron diffraction. [f] Ref 92 using X-ray diffraction.

systems of similar size (32 molecules) at various concentrations, the most dilute one (mole ratio 1:31) being comparable to ours. However, they focused on the dissociation and the effect of concentration and reported only little on structural properties. As far as comparison was possible, their results agree within the statistical error margins with our findings. Aqueous HCl solutions have also been studied by molecular simulation using (semi)empirical force fields. Here we can distinguish between simple nonpolarizable[51] and more advanced polarizable[52] water models. Note that the force-field studies considered solvation of a single Cl^-, leaving out the H^+ counterion. A comparison with our results is therefore only possible to a limited extent.

From Figure 3 and Table 5, we see that peak positions obtained with our AIMD simulations are shifted somewhat to smaller radii compared to those of the experiment and polarizable force-field MD simulation. Note also some enhanced structure of the second solvation shell, visible in the g_{Cl-O} distribution function beyond $r = 4$ Å and also in g_{Cl-O} beyond $r = 3.5$ Å. This structure is not present in the classical MD simulation. The observed differences need not be entirely due to the use of an ab initio (DFT) potential instead of an effective pair potential. It could also be attributed to the presence of the H^+ counterion that resides on average in the second solvation shell. A second factor could be the small size of the periodic simulation box contributing to some extra structuring.

The coordination numbers listed in Table 5 show that in our CP-PAW MD simulation Cl^- has on average five hydrogen bonds, in good agreement with the findings of the CP-MD simulation of ref 50 and the simulation with the advanced polarizable force field. Note that the nonpolarizable force field overestimates the coordination of the hydrogens significantly. The oxygen coordination number from our CP-PAW MD simulation of 7.2 exceeds the results of the polarizable force field simulation by 1.1. Also, the comparison with the experimental[53] range of 5.3−6.2 indicates an overestimate. The large value is due to the shoulder feature on the right of the first peak of the g_{Cl-O} radial distribution function. Inspections of snapshots indicates that the first solvation shell contains on average one water molecule that is not hydrogen bonded to the Cl^- ion. Again, this feature might be attributed to the presence of the H^+ cation in the second solvation shell.

The excess proton is associated with a single water molecule, forming H_3O^+ in approximately 70% of the time, and shared between two water molecules, forming a $H_5O_2^+$ complex in approximately 30% of the time. This is in agreement with the CP-MD results of Tuckerman et al.[4,5] from their study of the solvation and transport of H_3O^+ in water at infinite dilution with 60% and 40% abundancies of the H_3O^+ and $H_5O_2^+$ hydronium complexes, respectively. (See for the criteria to distinguishing between the complexes refs 4 and 5.) This difference might be attributed to the presence of the Cl^- ion in our work. The water structure surrounding the hydronium complexes is very similar to their results, which follows from the comparison of the radial distribution functions (data not shown).

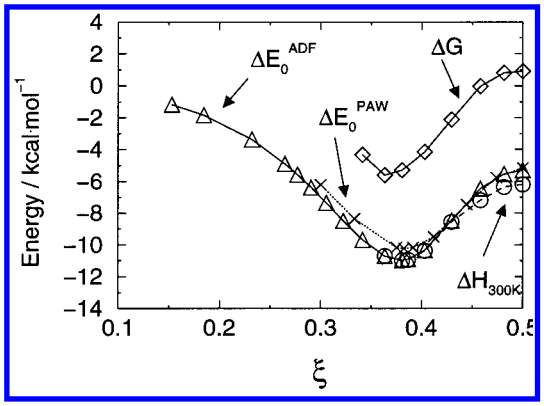

Figure 4. Energy profile for the gas-phase reaction calculated with ADF (triangles and solid line) and CP-PAW (crosses and dotted line). The zero-point energy and temperature contributions to the internal energy are very small at $T = 300$ K (ΔH_{300K}, circles and dashed line). Due to the much lower entropy of the reactant complex and transition state compared to that of the free reactants, the Gibbs free energy barrier $\Delta G = \Delta H - T\Delta S$ is much higher than the internal energy barrier (squares and solid line).]

From the calculations of the gas-phase structures and the preparatory CP-PAW MD simulations of water and dilute hydrochloric acid, we may conclude that our numerical approach, using DFT-BP together with the Car−Parrinello technique as implemented in the PAW method, yields results consistent with results reported in the literature. These results also confirm reports in the literature that the CP-MD method is able to reproduce properties of aqueous solutions with an acceptable accuracy. An important technical detail is that, for accuracies of 1 kcal/mol for the energies and 0.03 Å for bond lengths of the systems in this study, the plane wave basis set can be kept as small as a 30 Ry. kinetic energy cut off.

C. S_N2 Reaction in Gas Phase. To study the solvation effects on the reaction between CH_3Cl with Cl^-, we will first consider the gas-phase reaction. Starting with separated reactants, the reaction energy $\Delta E(\xi)$ decreases as the attacking chloride anion approaches the dipolar CH_3Cl from the carbon side to form a reaction complex, with complexation energy ΔE^{RC} (see Figure 4). Moving along to the product side, $\Delta E(\xi)$ increases until the reactants arrive at the D_{3h} symmetric transition state, with energy ΔE^{TS}. The product side of the profile is symmetric to the reactant side. The numerous attempts to estimate ΔE^{RC} and ΔE^{TS} have resulted, especially for the latter, in a variety of values for these quantities. A selection of these energies and the corresponding geometries found in the literature, as well as our own results are compiled in Table 6. For the ion−dipole reaction complex energy, the best ab initio number is probably given by the G2 calculation of Glukhovtsev et al: ΔE^{RC} kcal/mol.[10,54] Our DFT results and the ab initio and DFT results from literature are all within 1 kcal/mol to this number. Also the experimental estimate by Larson and McMahon agrees within their error estimate with this value. Only the CISD (configurational interaction, including single and double excitations) result by Vetter and Zülicke is about 2 kcal/mol too low.

The results for the transition-state energies, varying from −5.7 to 8.7 kcal/mol (see Table 6) have lead to a number of conflicting views. For instance, Streitwieser et al. (ref 13)

TABLE 6: Bonding Energy and Geometry of the Reaction Complex (RC) and the Transition State (TS) in Gas Phase at $T = 0$ K Compared to Other Methods

	reaction complex transition state			transition state		
	ΔE^{RC} [kcal/mol]	R_{CCl} [Å]	R_{CCL} [Å]	ΔE^{TS} [kcal/mol]	R_{CCl} [Å]	$\Delta E^{barrier}$ [kcal/mol]
CP-PAW/BP	−10.39	1.91	3.01	−5.32	2.37	5.1
ADF−BP	−10.96	1.88	3.09	−5.30	2.35	5.7
DFT-BP[a]	−10.3	1.835	3.098	−5.7	2.342	4.6
MP2[a]	−10.5	1.808	3.266	3.5	2.316	14.0
MP4[a]	−10.6			1.8		12.4
MP2[b]				4.01	2.28	
CCSD(T)[b]				2.65	2.301	
G2[c]	−10.51	1.810	3.270	2.76	2.317	13.26
DFT-B3LYP[d]	−9.72	1.858	3.180	1.1	2.371	10.8
HF/CISD[e]	−8.7	1.823	3.384	8.7	2.408	17.5
MP2[f]	−9.66	1.808	3.267	7.68	2.316	17.34
B3LYP[f]	−9.52			−0.85		8.67
Expt.	−8.6 ± 0.2[g]			1. ± 1.[h]		13.2 ± 2.2[h]
	−12.2 ± 2[i]					

[a] 1994 6-31G(d,p).[8] [b] Coupled-cluster calculations by Peter Botschwina.[9] At $T = 300$K, G2 method effectively becomes QCISD(T)/6-311+G(3df,2p) + ZPE correction for energies and MP2/6-311+G(3df,2p) for geometries.[10] [d] 6-311+G(3df,2p) basis set.[11] [e] Geometries using Hartree−Fock and energies using all electron CISD with Davidson correction and DZDP basis set quality.[12] [f] 1997 6-31G* basis set.[13] [g] High-pressure mass spectrometry.[14] [h] From measurement of the rate coefficient at temperatures above $T = 300$K using a flowing afterglow technique and a simplified modification of RRKM theory.[15] [i] Using ion cyclotron resonance.[16]

concluded: "the large differences in TS properties between MP2 and B3LYP suggest that the latter may not always be reliable for TS structures". And Deng et al. (ref 8) concluded that "the experimental data (for ΔE^{TS} and $\Delta E^{barrier}$) seem to fall in the region with the MP4 and NL-SCF (DFT-BP) value as the upper and lower bounds, respectively." The highest-level ab initio result for ΔE^{TS} is the CCSD(T) calculation by Botschwina, equal to 2.65 kcal/mol. The G2 estimate by Glukhovtsev et al. agrees very well with it, as well as the approximate experimental result of 1.0 ± 1.0 kcal/mol. This would imply that the DFT-BP result of −5.7 kcal/mol by Deng is just too low and underestimates ΔE^{TS} significantly. Streitwiesers MP2 result of 7.7 kcal/mol seems erroneous compared to the MP2 results of Botschwina (4.01 kcal/mol) and Deng et al (3.5 kcal/mol). The overestimation of the CISD energy (8.7 kcal/mol) is probably due to a combination of an inaccurate (HF) geometry and too small a basis set (DZDP).

There are indications that the too low transition-state energy by DFT-BP is systematic for structures with a symmetrical three-center four-electron bond, such as the σ-bond in Cl−C−Cl. For example, Gritsenko et al.[55] investigated the very similar $[F-CH_3-F]^-$ transition-state structure. They concluded that the delocalization of the exchange hole over the three atoms, in combination with a very small nondynamical correlation, is erroneously represented by the exchange part of the GGA density functional, which introduces a localized hole and thus a spurious nondynamical correlation.[55] This is, of course, important to keep in mind as we proceed to the S_N2 reaction in water solution. Anticipating the results for the reaction in aqueous solution, we may expect that the transition state in the solvated case is underestimated by an amount on the order of 8 kcal/mol because of the similarity in the geometric and electronic structure of the reacting species. The accuracy of the solvation effects should, in principle, be on the order of 1 kcal/mol, as determined from the simulations in the previous sections III.A and III.B.

Figure 4 plots the reaction energy profile, as well as the reaction enthalpy ΔH and the free energy ΔG. The latter two are calculated only between the reactant complex and the transition state because of the failure of the smooth change of vibrational contributions into translational and volume work contributions for further separated reactants. The total correction to the calculated energy ΔE_0 to obtain the enthalpy ΔH at a temperature of $T = 300$ K (see eq 3) is very small for the ion−dipole complex. It amounts to less than 0.1 kcal/mol for the equilibrium geometry and −0.9 kcal/mol for the transition state. This is in good agreement with the estimates by Vetter and Zülicke (0.1 kcal/mol and −0.5 kcal/mol, respectively). The formation of the ion−dipole complex from infinitely separated reactants involves a large negative entropy change, equal to $T\Delta S = -5.5$ kcal/mol. The entropy difference ($T\Delta S$) of the transition state with respect to the free reactants is −7.1 kcal/mol, which means that the intrinsic free energy reaction barrier is about 1.6 kcal/mol higher than the internal energy barrier.

D. S_N2 Reaction in Water. In this section, we will discuss the results of the constrained molecular dynamics simulations performed to study the $CH_3Cl + Cl^-$ reaction in a dilute aqueous solution of HCl. To obtain the free energy barrier ΔA, we calculated the mean force of constraint $\langle \partial H/\partial \xi \rangle_\xi$ at 5 points ($\xi = \{0.32, 0.35, 0.40, 0.45, 0.50\}$) along the reaction coordinate ξ (eq 2). As a verification of the simulations, $\langle \partial H/\partial \xi \rangle_\xi$ was also calculated at three points at the product side of the reaction coordinate ($\xi = \{0.55, 0.60, 0.70\}$). Subsequently, two extra simulations were performed for the point $\xi = 0.27$ (because at $\xi = 0.32$ there was still too large an attraction between CH_3Cl and Cl^- whereas for separated reactants $\langle \partial H/\partial \xi \rangle_\xi$ should be equal to zero) and at $\xi = 0.43$ (where we expected an extremum in $\langle \partial H/\partial \xi \rangle_\xi$).

The results for the mean force of constraint are plotted in Figure 5 (and listed in Table 8). The dashed line is a cubic spline fitted to the calculated points. Integration of the mean force of constraint with respect to ξ (according to eq A3) results in the free energy barrier, shown by the solid line in the figure, yielding a barrier height of 22.2 kcal/mol. If the 8 kcal/mol error in the gas-phase reaction is taken into account, the free energy barrier of the reaction in aqueous solution would be 30.2 kcal/mol, an overestimation of about 3.6 kcal/mol compared to the experimental result of 26.6 kcal/mol.[18]

Because of the symmetry of the reaction, the calculated energy profile should be symmetric. From the figure, it is obvious that the shape has a significant asymmetry. This asymmetry has been illustrated by asterisks in the figure. They have been drawn in Figure 5 above the three points at the product side of the reaction ($\xi = \{0.55, 0.60, 0.70\}$) to picture the equivalent points at the reactant side (with the negative force) for comparison. Moreover, the mean force of constraint does

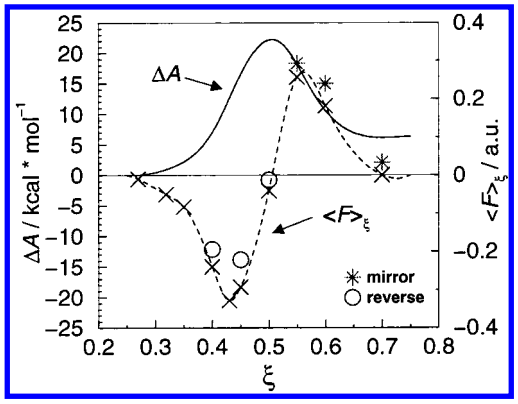

Figure 5. Mean force of constraint $\langle F\rangle_\xi$ (dashed line; right-hand-side axis) and the Helmholtz free energy ΔA (solid line; left-hand-side axis) vs the reaction coordinate ξ. The crosses denote the values from subsequent constrained MD runs, starting with a reaction coordinate value of $\xi = 0.270$. The circles are from subsequent runs in the backward reaction coordinate direction, starting from the finished run with $\xi = 0.55$. The three asterisks denote the points at $\xi = \{0.30,0.40,0.45\}$ mirrored in ($\xi = 0.5$, $F = 0$) to indicate the hysteresis. See also text.

TABLE 7: The Coordination Numbers of the Water Solvation Shells around the Attacking Cl^- and the Leaving Cl, at Different Points on the Reaction Coordinate[a]

	attacking chloride		leaving chloride	
ξ	$n_{c\,Cl'-H}$	$n_{c\,Cl'-O}$	$n_{c\,Cl-H}$	$n_{c\,Cl-O}$
0.27	5.4	6.3	–	–
0.32	4.3	5.1	–	–
0.35	4.9	4.6	–	–
0.40	4.7	4.4	–	–
0.43	4.8	4.8	–	–
0.45	4.2	4.5	1.1	4.4
0.50	3.3	4.3	2.7	(4.8)
0.50[b]	2.9	(5.6)	3.0	(4.3)
0.55	2.2	(4.8)	4.0	5.0

[a] The coordination numbers were calculated by integration over the peak in the radial distribution function (a hyphen indicates there was no such peak). Numbers between parentheses indicate that the peak was too broad for an accurate estimate. [b] Coming back from $\xi = 0.55$ (see text).

TABLE 8: Average Constraint Force for the Different Reaction Coordinate Values ξ

ξ	λ	$\langle Z^{-1/2}\lambda\rangle_\xi/\langle Z^{-1/2}\rangle_\xi$	$F(\xi)$
0.27	−0.0091	−0.0098	−0.0095
0.32	−0.0494	−0.0498	−0.0496
0.35	−0.0815	−0.0831	−0.0830
0.40	−0.2384	−0.2396	−0.2394
0.43	−0.3268	−0.3277	−0.3276
0.50	−0.0408	−0.0408	−0.0408
0.55	0.2570	0.2572	0.2571
0.60	0.1955	0.1966	0.1964
0.70	0.0018	0.0004	0.0002

[a] The constraint force is shown once as the Lagrange parameter λ, once corrected according to eq A1 and once more with the full correction according to eq A3.

not vanish at the transition state $\xi = 0.5$ as it should. The three product-side points as well as the point at the transition state apply to $[Cl\cdots CH_3\cdots Cl]^-$ configurations with a driving force that is smaller toward the product-side (or larger toward the reactant-side) than was expected from the other points at the reactant-side. This can be characterized as hysteresis when forcing the reaction by the method of constraint. Most likely, this hysteresis is due to the surrounding water shell, which apparently adapts too slowly to the changing reactants configuration, when going from one simulation to the next by increasing ξ.

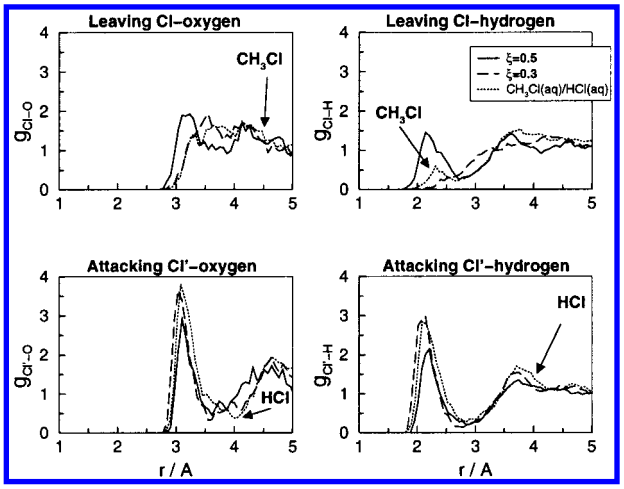

Figure 6. Radial distribution of water around the leaving Cl atom (upper graphs) and attacking Cl^- atom (lower graphs) for two points on the reaction coordinate, namely, $\xi = 0.5$ (the transition state: solid lines) and $\xi = 0.32$ (initial reactants: dashed lines). The graphs on the left-hand side show the distribution of the water oxygens and the right-hand side graphs the distribution of the water hydrogens. For comparison, dotted lines are drawn in for the g_{Cl-O} and g_{Cl-H} of CH_3Cl in water (upper graphs) and HCl in water (lower graphs).

To test this explanation, we performed calculations for the reversing of the reaction. We performed the backward reaction for three points ($\xi = \{0.50, 0.45, 0.40\}$), where we started from the constrained MD run at $\xi = 0.55$ and moved the constraint value slowly to the previous point on the reaction coordinate. Subsequently, we equilibrated for 2.5 ps, collected the force of constraint for 3 ps, and moved on to the next point, similar to the points of the forward reaction direction. The results are shown by the circles in Figure 5. The hysteresis at the first point, $\xi = 0.50$, has disappeared since $\langle F(0.5)\rangle_\xi$ is zero (within the error in the force), as expected. Apparently, the solvent configuration is not pulling on either side of the reacting complex at this point. For the other two points, we now find smaller absolute values for the mean force of constraint than we found in the forward reaction. This is consistent with the picture of a "memory effect" in the solvent, i.e. a too slow adaptation of the water configuration to the changed reaction coordinate.

A rough estimate of the systematic error on the free energy barrier due to the hysteresis can be made by assuming that the deviation in the force will increase linearly from zero at the starting point of the separate reactants ($\xi \approx 0.25$) to the observed −0.041 au at the transition state. Correcting the free energy profile for the corresponding overestimation (3.2 kcal/mol) gives a barrier height of 27 kcal/mol. The excellent agreement with experiment (26.6 kcal/mol) after the corrections for the DFT-GGA error in the gas-phase transition-state energy and the hysteresis in the constrained MD runs must be a bit fortuitous for the following reasons. First of all, we have found the accuracy of the DFT-BP description of the energetics of the solvation to be on the order of 1 kcal/mol. Second, the experimental result refers to more dilute solution at neutral pH, with typically potassium used for the countercation. In the present calculation, a proton acted as countercation, which can be expected to have some influence on the energetics of the reaction via its charge and solvation structure.

Next, we turn to the structural aspects of the reaction. In Figure 6, we compare the radial distribution functions of the

water atoms with respect to the leaving and attacking chloride ions, calculated for the transition state and for the more separated reactants ($\xi = 0.32$). From integration over the first peak of the distribution functions, the coordination numbers for the chloride ions were calculated and compiled in Table 7 (for all simulated values of ξ).

To start with the separated reactants at $\xi = 0.32$, we note that the distribution functions $g_{Cl'-O}$ and $g_{Cl'-H}$ of the attacking chloride anion (dashed lines in the lower graphs) are very similar to the functions of pure HCl in water (dotted lines; see also Figure 3). The distribution around the leaving chloride atom at $\xi = 0.32$ (upper two graphs) is in agreement with pure CH_3Cl in water (dotted lines), except for a small peak in g_{Cl-H} at $r = 2.3$ Å in the latter. The small peak in the pure CH_3Cl solution (case b in section II-D) can be attributed to one water molecule which is hydrogen bonded to the Cl of methyl chloride. The main reason for the absence of this peak in g_{Cl-H} of the leaving Cl must be the presence of the Cl^- anion, which has a strong influence on the solvent structure. The coordination numbers (in Table 7) shows that the attacking chloride anion is solvated by about five water molecules, whereas the separate CH_3Cl does not show any attraction of water atoms. Note that $n_{c\,Cl'-H}(\xi = 0.32) = 4.3$ confirms that this starting constrained simulation indeed does not fully resemble separated reactants as concluded in section III.D, whereas the extra simulation of $\xi = 0.27$ shows coordination numbers of 5.4 and 6.3, in agreement with the values for the pure HCl in water (5.2 and 6.5, Table 5).

Next, we discuss the radial distribution functions for the transition-state configurations (solid lines). These show a more equal solvation of the attacking and leaving chloride ions. However, the first peaks of the attacking chloride ion are still much more pronounced than the peaks arising from the first solvation shell around the leaving chloride. Also, the minimum at $r = 3.5$ Å is much deeper in $g_{Cl'-O}$ than that in g_{Cl-O}. This asymmetry in the chloride solvation is reflected less strongly in the coordination numbers (Table 5). The attacking chloride still has on average 3.3 hydrogens in the first shell, while the leaving chloride has only 2.7. The Cl−O coordination numbers cannot be determined accurately because the oxygen distribution function g_{Cl-O} of the leaving Cl does not show an unambiguous minimum. Still, from the hydrogen distribution, we can conclude that the attacking Cl is stronger solvated than the leaving Cl at $\xi = 0.5$, which must be the grounds for the effective force of constraint at the transition state. Indeed, in the reversed reaction direction, where we found the expected $\langle F(0.5)\rangle_\xi = 0$, we also see a more symmetric hydrogen distribution (radial distribution functions not shown) and coordination numbers of 2.9 for the attacking Cl and 3.0 for the leaving Cl. Just before the transition state, the leaving chloride has only one hydrogen in the "first shell" ($n_{c\,Cl-H}(\xi = 0.45) = 1.1$), whereas just after the transition state, the attacking chloride still has two hydrogens ($n_{c\,Cl'-H}(\xi = 0.55) = 2.2$). This difference leads to a larger value for the mean force of constraint at $\xi = 0.45$ in comparison with $\xi = 0.55$ and gives a structural explanation for the observed hysteresis in the free energy profile of Figure 5.

IV. Discussion

The present results show that Car−Parrinello MD simulation is a powerful tool to assess solvent effects on a simple S_N2 reaction. Semiquantitative results for the energetics and a detailed picture of the structural aspects of the reaction are obtained. However, the study also shows that at present time the calculations are not without limitations. The most important ones, the relatively small box size and the short trajectories that can be calculated, cannot easily be removed because they are related to the high computational expense. For example, the time necessary to calculate one point from Figure 5 (say, 6 ps total time for equilibration and sampling) was about 11 days on 6 IBM-SP nodes (power2sc processor) or 29 days on a cluster of 16 IBM RS6000 43P workstations.

The hysteresis found in the force of constraint is due to a memory effect in the solvent, which is directly related to the fact that the last configuration of every constrained MD run is used to construct the initial configuration for the simulation at the next point of the reaction coordinate, in combination with the limited time scale accessible to a AIMD simulation. Apparently, the rearrangements that have to be made by the solvent, to follow the change in the reaction coordinate from point to point, occur on a much longer time scale than the rotations and vibrations and diffusion of water molecules that are well described by our 10 ps molecular dynamics trajectories.

Simulating for longer times is the trivial solution to avoid memory effects. However, this could be as impractical as waiting for the reaction to occur spontaneously because there are indications that the adaptation of the aqueous solvent to the changing solute configurations is an activated process instead of a slowly diffusive process. In the 9 ps transition-state simulation, for instance, a drift in the force of constraint would be expected, which should asymptotically decay toward zero in the case of a slowly diffusively adapting solvation shell, but was not observed. Nor in the next 10.2 ps run at $\xi = 0.55$ (or in any of the other constrained MD runs) did we find a drift in the force, which means that the solvent adaptation responsible for the correct zero force at $\xi = 0.5$ in the reversed reaction direction must have taken place in the short time when the constraint was moved from $\xi = 0.5$ to $\xi = 0.55$. This indicates that a solvent rearrangement has been able to overcome a small free energy barrier when the system was forced to the next reaction coordinate configuration.

Second, we note that the force-field Monte Carlo simulations of the same S_N2 reaction in 250 water molecules by Chandrasekhar et al,[17] using the umbrella sampling technique, also shows a significant hysteresis. The calculated probability distribution $P(\xi = \xi_{TS})$ (figure 5 in ref 17) is not symmetric: the second peak at the reactant side next to the transition state is absent at the product side. This is also reflected in the radial distribution functions obtained from the MC simulation of the transition state.

It has become clear that certain necessary changes in the solvent as the reaction takes place are rare events on the typical AIMD time scales. One way to handle the problem of hysteresis is therefore to include the required solvent rearrangements into the reaction coordinate. Unfortunately, due to the large number of molecules involved and their complex rearrangements, finding a proper reaction coordinate is virtually impossible. The need to include solvent degrees of freedom into the reaction coordinate was also concluded recently by Geissler, Dellago, and Chandler from their molecular simulations of the dissociation of NaCl in water.[56] In this work, they found additional free energy barriers in the solvent that have to be overcome as the reaction (i.e. the dissociation) occurs. For instance, the addition of a water molecule in the first solvation shell of Na^+ to bring the coordination from the initial 5-fold to the final 6-fold required an amount of work equal to $1.7k_BT$ (~1 kcal/mol)). During the S_N2 reaction in the present work, a Cl^- solvation shell has to lose two water molecules to reach the transition state, while at the same time, the CH_3Cl chloride has to bond

with three water molecules which have to be taken from the water network.

V. Conclusions

Using the Car−Parrinello method, we studied the solvation effects on the identity reaction between Cl^- and CH_3Cl in a dilute (1:32 mole ratio) aqueous solution of HCl. We compared the free energy profile of the reaction in the gas phase and in solution and analyzed the structure of the solution at different stages of the reaction. The free energy profile of the reaction in aqueous solution was obtained using the method of constrained molecular dynamics simulations in combination with thermodynamic integration. The calculated barrier yields 27 kcal/mol after application of certain corrections (see below). This corrected value is in good agreement with the experimental value of 26.6 kcal/mol.

There are two important error sources in these calculations. The DFT (Becke−Perdew functional) electronic structure calculations describe the solvent and the solvent−solute interactions, in particular the solvation of the Cl^- ion, the formation of the initial ion−dipole complex of Cl^- with CH_3Cl, and the solvation of the reaction system in the course of the reaction, with reasonable accuracy. However, although DFT-BP does exhibit an energy rise when going from the ion−dipole complex to the transition state, thus reproducing the well-known double-well energy profile for the gas-phase reaction, it underestimates the barrier height of ca. 13 kcal/mol by as much as 8 kcal/mol. This error, being related to an imbalance in the description of exchange and correlation in the transition state by present-day generalized gradient approximations such as Becke−Perdew, cf. ref 55, will persist in the transition state in solution. A correction of 8 kcal/mol has therefore been applied to the calculated barrier height. In the second place, a "hysteresis", or inequivalence of forward and reverse reaction, has been found in the force of constraint profile. The hysteresis is due to a slow adaptation of the solvent to the reacting solutes and has the effect of pulling the reactants back toward the initial state when the constrained reaction coordinate is moved toward the product side. Apparently, the rearrangements that have to be made by the solvent occur on a much longer time scale than those of the rotations and vibrations and self-diffusion of water molecules that are well described by our 10 ps molecular dynamics trajectories. On the time scale of MD simulations, the rearrangements needed in the solvation shells of the reactants are rare events by themselves. Including solvent degrees of freedom in the reaction coordinate is in principle the way to handle this type of the rare events.[56]

The Car−Parrinello MD simulation of the reactants in a box with 32 water molecules is an important improvement on the numerous microsolvation and dielectric continuum calculations. It is a great advantage that the varying solvation during the course of the reaction, due to the shift of negative charge from the attacking chloride initially to the leaving chloride finally, does not have to be described by parametrized model potentials that cannot be optimal for all occurring situations along the reaction coordinate. From the good agreement with experiment—after the corrections described above—we may infer that both the energetic and the entropic effects of the solvation on the free energy barrier are obtained to quite satisfactory accuracy with the AIMD simulation. Further improvements of this type of calculation can be envisaged, of both technical and more fundamental nature. At the technical side, we note that the limited size of the total system implies that approximations are made on the long-range interactions in the solvent. Also, the fixed volume has a small effect on the forces because the changing size of the reaction complex in solution affects the pressure on the system. The extension of the present type of calculation to larger systems will certainly be possible in the future due the rapid increase in available computing power. The most important deficiencies of the present work are of a more fundamental nature. The first is the underestimation of the transition-state energy by the GGA (Becke−Perdew) functional. This will have to be remedied by the development of more accurate functionals, which, in view of computation time, should not rely on the incorporation of exact exchange. In the second place, it is desirable that the dynamics methods are improved in order to keep the necessary simulation times down to a manageable length. One possibility would be the development of methods to handle the slow adaptation of the solvent structure to the changing reaction coordinate by incorporating the necessary change in solvent structure in the reaction coordinate.

Acknowledgment. B.E. and E.J.M. gratefully acknowledge the support by the Prioriteits Programma Materialen-Computational Materials Science (PPM-CMS). We thank the foundation NCF of The Netherlands Foundation for Scientific Research (NWO) for computer time. E.J.M. acknowledges the "Royal Netherlands Academy of Arts and Sciences" for financial support.

Appendix A. Force of Constraint

The system can be constrained to a hyperplane $\xi(\mathbf{r}) = \xi'$ in phase space in a molecular simulation by extending the Lagrangian with a term $\lambda(\xi(\mathbf{r}) - \xi')$, with $\mathbf{r}$ being the atomic positions, ξ our reaction coordinate, and λ the Lagrange multiplier associated with the force on the holonomic constraint. Each atom i then feels a constraint force equal to $F_i(\xi) = \lambda(\mathrm{d}\epsilon/\mathrm{d}r_i)$. It is well-known that the use of constraints affects the phase space distribution (see, e.g., ref 31). For a velocity-independent property p, the bias introduced by a constraint can be compensated using the relation

$$\langle p(\mathbf{r})\rangle^{\mathrm{unconstr}} = \frac{\langle Z^{-1/2} p(\mathbf{r})\rangle_\xi}{\langle Z^{-1/2}\rangle_\xi} \tag{A1}$$

where the factor Z is defined by

$$Z = \sum_i \frac{1}{m_i}\left(\frac{\partial \xi}{\partial \mathbf{r}_i}\right)^2 \tag{A2}$$

This was generalized recently for velocity-dependent properties, such as the mean force of constraint.[37,38] In the formulation of ref 37, it reads

$$F(\xi) = \frac{\langle \lambda_\xi Z^{-1/2}\rangle_\xi + \frac{1}{2}k_B T\left\langle Z_\xi^{-5/2}\sum_{i=1}^{N}\frac{1}{m_i}\nabla_i\xi\cdot\nabla_i Z\right\rangle_\xi}{\langle Z^{-1/2}\rangle_\xi} \tag{A3}$$

where T is the temperature, k_B is Boltzmann's constant, and m_i is the mass of particle i.

The second term in the numerator of equation A3 arises because the mean force of constraint depends on the velocities through the kinetic term $\partial K/\partial\xi$ in the force of constraint (eq 1). In their work, they demonstrated the importance of the corrections for a constrained bending angle of a triatomic molecule and for a constrained dihedral angle in a tetra atomic molecule.

In Table 8, we show the results for the mean force of constraint for our S_N2 reaction using the constraint of eq 2, once as λ, once corrected according to equation A1, and once using eq A3. As the differences are very small, the bias on our system introduced by the constraint must by very small.

References and Notes

(1) Car, R.; Parrinello, M. *Phys. Rev. Lett.* **1985**, *55*, 2471.
(2) Laasonen, K.; Sprik, M.; Parrinello, M. *J. Chem. Phys.* **1993**, *99*, 9080.
(3) Sprik, M.; Hutter, J.; Parrinello, M. *J. Chem. Phys.* **1996**, *105*, 1142.
(4) Tuckerman, M.; Laasonen, K.; Sprik, M.; Parrinello, M. *J. Phys. Chem.* **1995**, *99*, 5749.
(5) Tuckerman, M.; Laasonen, K.; Sprik, M.; Parrinello, M. *J. Chem. Phys.* **1995**, *103*, 150.
(6) Meijer, E. J.; Sprik, M. *J. Phys. Chem. A* **1998**, *102*, 2893.
(7) Meijer, E. J.; Sprik, M. *J. Am. Chem. Soc.* **1998**, *120*, 6345.
(8) Deng, L.; Branchadell, V.; Ziegler, T. *J. Am. Chem. Soc.* **1994**, *116*, 10645.
(9) Botschwina, P. *Theor. Chem. Acc.* **1998**, *99*, 426.
(10) Glukhovtsev, M. N.; Pross, A.; Radom, L. *J. Am. Chem. Soc.* **1995**, *117*, 2024.
(11) Glukhovtsev, M. N.; Bach, R. D.; Pross, A.; Radom, L. *Chem. Phys. Lett.* **1996**, *260*, 558.
(12) Vetter, R.; Zülicke, L. *J. Am. Chem. Soc.* **1990**, *112*, 5136.
(13) Streitwieser, A.; Choy, G. S.; Abu-Hasanayn, F. *J. Am. Chem. Soc.* **1997**, *119*, 5013.
(14) Dougherty, R. C.; Dalton, J.; Roberts, J. D. *Org. Mass. Spectrosc.* **1973**, *8*, 77.
(15) Barlow, S. E.; van Doren, J. M.; Bierbaum, V. M. *J. Am. Chem. Soc.* **1988**, *110*, 7240.
(16) Larson, J. W.; McMahon, T. B. *J. Am. Chem. Soc.* **1985**, *107*, 766.
(17) Chandrasekhar, J.; Smith, S. F.; Jorgensen, W. L. *J. Am. Chem. Soc.* **1985**, *107*, 154.
(18) Albery, W. J.; Kreevoy, M. M. *Adv. Phys. Org. Chem.* **1978**, *16*, 87.
(19) Carter, E. A.; Ciccotti, G.; Hynes, J. T.; Kapral, R. *Chem. Phys. Lett* **1989**, *156*, 472.
(20) Parr, R. G.; Yang, W. *Density-Functional Theory of Atoms and Molecules*; Oxford University Press: New York, 1989.
(21) Perdew, J. P.; Zunger, A. *Phys. Rev. B* **1981**, *23*, 5048.
(22) Ceperley, D. M.; Alder, B. J. *Phys. Rev. Lett.* **1980**, *45*, 566.
(23) Becke, A. D. *J. Chem. Phys.* **1992**, *96*, 2155.
(24) Perdew, J. P. *Phys. Rev. B* **1986**, *33*, 8822.
(25) Verlet, L. *Phys. Rev.* **1967**, *159*, 98.
(26) Nosé, S. J. *J. Chem. Phys.* **1984**, *81*, 511.
(27) Blöchl, P. E. *Phys. Rev. B* **1994**, *24*, 17953.
(28) Petrilli, H. M.; Blöchl, P. E.; Blaha, P.; Schwarz, K. *Phys. Rev. B* **1998**, *57*, 14690.
(29) Blöchl, P. E. *Phys. Rev. B* **2000**, in press
(30) Baerends, E.; Ellis, D.; Ros, P. *Chem. Phys.* **1973**, *2*, 41.
(31) Frenkel, D.; Smit, B. *Understanding Molecular Simulation*; Academic: San Diego, CA, 1996.
(32) Chandler, D. *J. Chem. Phys.* **1978**, *68*, 2959.
(33) van Gunsteren, W. F. In *Computer Simulations of Biomolecular Systems: Theoretical and Experimental Applications*; van Gunsteren, W. F., Weiner, P. K., Eds.; ESCOM: Leiden, The Netherlands, 1989; Vol. 1.
(34) Ryckaert, J. P.; Ciccotti, G.; Berendsen, H. J. C. *J. Comput. Chem.* **1977**, *23*, 327.
(35) Neria, E.; Fischer, S.; Karplus, M. *J. Chem. Phys.* **1996**, *105*, 1902.
(36) Margl, P.; Lohrenz, J. C. W.; Ziegler, T.; Blöchl, P. E. *J. Am. Chem. Soc.* **1996**, *118*, 4434.
(37) den Otter, W. K.; Briels, W. J. *J. Chem. Phys.* **1998**, *109*, 4139.
(38) Sprik, M.; Ciccotti, G. *J. Chem. Phys.* **1998**, *109*, 7737.
(39) Blöchl, P. E. *J. Chem. Phys.* **1995**, *103*, 7422.
(40) Atkins, P. W. *Physical Chemistry*; Oxford University Press: New York, 1990.
(41) MP2 limit estimates: Feyereisen et al., -4.9 ± 0.1[57]; Schütz et al., -4.94 ± 0.02[58]; Xantheas, -4.9[59]; Hobza et al., -5.029[60]; Halkier et al., -4.94 ± 0.1[42]; Klopper et al., -4.99.
(42) Halkier, A.; Koch, H.; rgensen, P. J.; Christiansen, O.; Nielsen, I. M. B.; Helgaker, T. *Theor. Chim. Acta* **1997**, *97*, 150.
(43) Kim, K.; Jordan, K. D. *J. Phys. Chem.* **1994**, *98*, 10089.
(44) Proynov, E. I.; Sirois, S.; Salahub, D. R. *Int. J. Quantum Chem.* **1997**, *64*, 427.
(45) Becke, A. D. *Phys. Rev. A* **1988**, *38*, 3098.
(46) Perdew, J. P.; Wang, Y. *Phys. Rev. B* **1986**, *33*, 8800.
(47) Combariza, J. E.; Kestner, N. R. *J. Phys. Chem.* **1995**, *99*, 2717.
(48) Krynicki, K.; Green, C. D.; Sawyer, D. W. *Faraday Discuss. Chem. Soc.* **1978**, *66*, 199.
(49) Laasonen, K.; Klein, M. L. *J. Am. Chem. Soc.* **1994**, *116*, 11620.
(50) Laasonen, K.; Klein, M. L. *J. Phys. Chem. A* **1997**, *101*, 98.
(51) Chandrasekhar, J.; Spellmeyer, D. C.; Jorgensen, W. L. *J. Am. Chem. Soc.* **1984**, *106*, 903.
(52) Sprik, M.; Klein, M. L.; Watanabe, K. *J. Phys. Chem.* **1990**, *94*, 6483.
(53) Enderby, J. E.; Cummings, S.; Herdman, G. J.; Neilson, G. W.; Salmon, P. S.; Skipper, N. *J. Phys. Chem.* **1987**, *91*, 5851.
(54) This value includes the zero-point energy, which we estimated with DFT-BP to be $\Delta E_{ZPE}^{RC} < |-0.1|$ kcal/mol.
(55) Gritsenko, O. V.; Ensing, B.; Schipper, P. R. T.; Baerends, E. J., to be published.
(56) Geissler, P. L.; Dellago, C.; Chandler, D. *J. Phys. Chem. B* **1999**, *103*, 3706.
(57) Feyereisen, M. W.; Feller, D.; Dixon, D. *J. Phys. Chem.* **1996**, *100*, 2993.
(58) Schütz, M.; Brdarski, S.; Widmark, P. O.; Lindh, R.; Karlström, G. *J. Chem. Phys.* **1997**, *107*, 4597.
(59) Xantheas, S. S. *J. Chem. Phys.* **1996**, *104*, 8821.
(60) Hobza, P.; Bludski, O.; Suhai, S. *Phys. Chem. Chem. Phys.* **1999**, *1*, 3073.
(61) Curtiss, L. A.; Raghavachari, K.; Redfern, P.; Pople, J. A. *J. Chem. Phys.* **1997**, *106*, 1063.
(62) Pople, J. A.; Head-Gordon, M.; Raghavachari, D. J. F. K.; Curtiss, L. A. *J. Chem. Phys.* **1989**, *90*, 5622.
(63) Curtiss, L. A.; Jones, C.; Trucks, G. W.; Raghavachari, K.; Pople, J. A. *J. Chem. Phys.* **1990**, *93*, 2537.
(64) In *Tables of Interatomic Distances and Configuration in Molecules and ions*; Sutton, L., Eds.; The Chemical Society: London, 1965.
(65) Callomon, J. H.; Hirota, E.; Kuchitsu, K.; Lafferty, W. J.; Maki, A. G.; Pote, C. S. In *Structure Data of Free Polyatomic Molecules*; Landolt-Börnstein New Series, Group II; Hellwege, K. H., Hellwege, A. M., Eds.; Springer: Berlin, 1976; Vol. 7.
(66) Huber, K. P.; Herzberg, G. In *Molecular Spectra and Molecular Structure IV: Constants of Diatomic Molecules*; Van Nostrand Reinhold: New York, 1979.
(67) Harmony, M. D.; Laurie, V. W.; Kuczkowski, R. L.; Schwendeman, R. H.; Ramsay, D. A.; Lovas, F. J.; Lafferty, W. J.; Maki, A. G. *J. Phys. Chem. Ref. Data* **1979**, *8*, 619.
(68) Tuma, C.; Boese, A. D.; Handy, N. C. *Phys. Chem. Chem. Phys.* **1999**, *1*, 3939.
(69) Mok, D. K. W.; Handy, N. C.; Amos, R. D. *Mol. Phys.* **1997**, *92*, 667.
(70) Klopper, W.; Lüthi, H. P. *Mol. Phys.* **1999**, *96*, 559.
(71) Xantheas, S. S.; Dunning, T. H. *J. Chem. Phys.* **1993**, *99*, 8774.
(72) Bentwood, R. M.; Barnes, A. J.; Thomas, W. J. O. *J. Mol. Spectrosc.* **1980**, *84*, 391.
(73) Odutola, J. A.; Dyke, T. R. *J. Chem. Phys.* **1980**, *72*, 5062.
(74) Curtiss, L. A.; Frurip, D. L.; Blander, M. *J. Chem. Phys.* **1979**, *71*, 2703.
(75) Reimers, J. J.; Watts, R. O.; Klein, M. L. *Chem. Phys.* **1982**, *64*, 9.
(76) van Duijneveldt-van der Rijdt, J. G. C. M.; van Duijneveldt, F. B. *J. Chem. Phys.* **1992**, *97*, 5019.
(77) Dunbar, R. C.; McMahon, T. B.; Thölmann, D.; Tonner, D. S.; Salahub, D. R.; Wei, D. *J. Am. Chem. Soc.* **1995**, *117*, 12819.
(78) Xantheas, S. S. *J. Phys. Chem.* **1996**, *100*, 9703.
(79) Hiraoka, K.; Mizuse, S.; Yamabe, S. *J. Phys. Chem.* **1988**, *92*, 3943.
(80) Sieck, L. W. *J. Phys. Chem.* **1985**, *89*, 5552.
(81) Yamabe, S.; Furumiya, Y.; Hiraoka, K.; Morise, K. *Chem. Phys. Lett.* **1986**, *131*, 261.
(82) In *CRC Handbook of Chemistry and Physics*; Lide, D. R., Ed.; Chemical Rubber: Boca Raton, Fl, 1994.
(83) Jorgensen, W. L.; Chandrasekhar, J.; Madura, J. D.; Impey, R. W.; Klein, M. L. *J. Chem. Phys.* **1983**, *79*, 926.
(84) van der Stoel, D.; van Maaren, P. J.; Berendsen, H. J. C. *J. Chem. Phys.* **1998**, *108*, 10220.
(85) Watanabe, K.; Klein, M. L. *Chem. Phys.* **1989**, *131*, 157.
(86) Liu, Y.; Ichiye, T. *J. Phys. Chem.* **1996**, *100*, 2723.
(87) Chandra, A.; Ichiye, T. *J. Chem. Phys.* **1999**, *111*, 2701.
(88) Tromp, R. H.; Posterino, P.; Neilson, G. W.; Ricci, M. A.; Soper, A. K. *J. Chem. Phys.* **1994**, *101*, 6210.
(89) Narten, A. H.; Danford, M. D.; Levy, H. A. *Discuss. Faraday Soc.* **1967**, *43*, 97.
(90) Narten, A. H.; Levy, H. A. *J. Chem. Phys.* **1971**, *55*, 2263.
(91) Newsome, J. R.; Neilson, G. W.; Enderby, J. E. *J. Phys. C: Solid State Phys.* **1980**, *923*, 13.
(92) Enderby, J. E.; Neilson, G. W. *Rep. Prog. Phys.* **1981**, *44*, 38.